

Jet Production in Deep-inelastic Scattering at HERA

Tancredi Carli

*Max-Planck-Institut für Physik, Werner-Heisenberg-Institut
Föhringer Ring 6, D-80805 München, Germany,
E-mail: h01rtc@rec06.desy.de*

*Invited talk given at the workshop 'New Trends in HERA Physics',
Schloss Ringberg, Tegernsee (Germany), May 1997.
On behalf of the H1 and ZEUS collaborations.*

ABSTRACT

The main experimental results on jet production at HERA are reviewed. A study of jet shapes shows that the internal structure of jets is well understood. The potential to accurately determine the strong coupling constant using jet rates is discussed. First attempts to extract the gluon density in next-to-leading order are presented. Although fixed order perturbative QCD is able to describe the shape of most variables associated to the hard subprocess leading to jets, it does not reproduce the absolute dijet rate over a large phase space region.

1. Introduction

HERA colliding 27.5 GeV positrons on 820 GeV proton offers an ideal testing ground for perturbative QCD in deep-inelastic scattering (DIS).

Hard processes can be investigated as function of a variable scale, such that the transition from one phase space region to another or the interplay between two hard scales, like e.g. the photon virtuality Q^2 or the transverse energy of a parton, can be studied. The center of mass energy of $\sqrt{s} \approx 300$ GeV leads to a large phase space for hadron production and to the possibility to observe clean 'jets' in the hadronic final state.

Jets are event properties relating the unobservable quarks and gluons to the measurable hadronic final state. Quantitative studies of jets require an exact definition of how to combine the spray of hadrons observed in the detector to jets. The definition should be suitable for the experimental analysis and for the theoretical calculation. Moreover, it should lead to infrared and collinear safe results, which do not change, if a low energetic particle is added or if a particle is split into two. Jets are usually defined either by cone type algorithms maximizing the transverse energy flowing through a cone in the (η, ϕ) plane^a or by algorithms successively recombining closest particles. Clustering algorithms iteratively merge pairs of particles until only a few well separated objects are left. The decision to assign a given object to a jet is based on a distance measure d_{ij} and a resolution parameter $y_{cut} = d_{ij}/\text{scale}$. Table 1

^a The pseudo-rapidity is $\eta = -\ln \tan(\theta/2)$, where θ is defined with respect to the incident proton. The proton defines the negative z axis. ϕ is the azimuthal angle.

Name	distance measure d_{ij}	scale	remnant treatment
JADE	$2E_i E_j (1 - \cos \theta_{ij})$	W^2	$\sum_h E - P_z$
W	$(p_i + p_j)^2$		
K_T	$2 \min(E_i^2, E_j^2) (1 - \cos \theta_{ij})$	Q^2 or fixed E_T^2	$d_{ip} = 2 E_i^2 (1 - \cos \theta_i)$
long.inv. K_T	$2 \min(E_{Ti}^2, E_{Tj}^2) (\Delta \eta_{ij}^2 + \Delta \phi_{ij}^2)$		$d_{ip} = 2 E_{Ti}^2$
scheme	E or JADE	P	E_0
combination procedure	$p_k = p_i + p_j$	$E_k = \vec{p}_i + \vec{p}_j $ $\vec{p}_k = \vec{p}_i + \vec{p}_j$	$E_k = E_i + E_j$ $\vec{p}_k = (E_i + E_j) (\vec{p}_i + \vec{p}_j) / (\vec{p}_i + \vec{p}_j)$

Fig. 1. Summary of the main characteristics of popular jet clustering algorithms. For the K_T algorithm the remnant is considered as a particle p with infinite momentum. In the JADE and W algorithm a pseudo-particle with longitudinal components calculated from the hadrons in the final state is introduced to account for the remnant. The combination procedure defines how the four-momentum $p_i = (E_i, \vec{p}_i)$ of two objects i and j are combined to an object k .

summarizes choices for commonly used clustering algorithms. Also shown are various procedures for the addition of particle 4-momenta to obtain the jet four-momentum (recombination schemes).

Traditionally cone algorithms have been applied in $p\bar{p}$ collisions where special care has to be taken to separate particles belonging to the beam remnant from particles associated with the hard subprocess. Cone algorithms are invariant under longitudinal boosts. In e^+e^- collisions, where the initial state is free of color charges and where every particle can be assigned to jets, clustering algorithms have been used. In DIS or $p\bar{p}$ collisions they can also be used if an additional particle to mimic the hadron remnant is put in by hand.

At HERA, events with two jets in the central part of the detector plus the jet associated with the proton remnant (2 + 1 jet events) can be produced in a quark ($q\gamma \rightarrow qg$) or a gluon ($g\gamma \rightarrow q\bar{q}$) initiated hard subprocess (see Fig. 2). The 2 + 1 jet cross section is given by¹:

$$\frac{d^2\sigma_{2+1}}{dx dQ^2} \sim \alpha_s(\mu_r) \int \frac{d\xi}{\xi} (C_{qg}(x/\xi, z_q, x, Q^2) \cdot q(\xi, \mu_f^2) + C_{q\bar{q}}(x/\xi, z_q, x, Q^2) \cdot g(\xi, \mu_f^2)) \quad (1)$$

where α_s is the strong coupling constant, μ_r the renormalisation and μ_f the factorisation scale. x and Q^2 are the usual variables to inclusively describe deep-inelastic scattering (see Fig. 2 for definition). The coefficient functions $C_{q\bar{q}}$ and C_{qg} can be calculated in perturbative QCD. In addition to x and Q^2 they depend^b on the two variables ξ and z_q characterizing the short distance subprocess which is responsible for the dijet system. The fraction of the longitudinal proton momentum carried by the incoming parton ξ , can be calculated in leading order α_s (LO) from the invariant mass of the jet system $\sqrt{\hat{s}}$:

$$\xi = x (1 + \hat{s}/Q^2) \quad (2)$$

^bThe dependence of C_{qg} and $C_{q\bar{q}}$ on the azimuthal angle ϕ between the lepton and the parton scattering plane is not given in the formula.

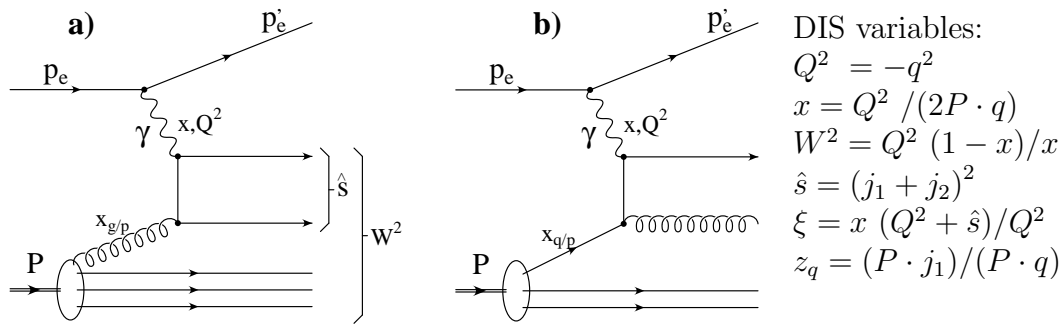


Fig. 2. Feynman diagrams for the production of 2 + 1 jet events to first order of α_s in ep -collisions. q (P) denote the four-momentum of the photon (proton). j_1 (j_2) is the four-momentum of one of the jets associated to the hard subprocess.

The variable z_q is given by:

$$z_q = \frac{P \cdot j_1}{P \cdot q} \approx \frac{1}{2}(1 - \cos \theta^*) \approx \frac{E_j(1 - \cos \theta_j)}{\sum_{j=1,2} E_j(1 - \cos \theta_j)} \quad (3)$$

where q (P) is the 4-momentum of the photon (proton) and θ^* is the polar angle^c of one of the jets with 4-momentum j_1 in the photon-parton center of mass frame. E_j and θ_j are the energy and polar angle of the jets in the laboratory frame. The parton distribution functions in the proton $q(\xi, Q^2)$ and $g(\xi, Q^2)$ absorb the collinear and infrared singularities which occur in the calculations of C_{qq} and C_{qg} , and they have to be extracted from experiments. Once measured at some scale Q_0^2 , they can be perturbatively evolved to any other scale, e.g. Q^2 , using the DGLAP equations². By convoluting them with the appropriate coefficient functions, they can be used to calculate the cross section in any other process. In this sense they are universal.

In leading order of α_s , the coefficient functions diverge like $C_{q\bar{q}} \sim 1/(z_q(1 - z_q))$ and $C_{qg} \sim 1/((1 - x/\xi)(1 - z_q))$ and have to be regulated by a cut-off. In Fig. 3 is shown how the cross section $d^2\sigma/dx_p dz_q$ (where $x_p = x/\xi$) increases towards low z_q and x_p and towards $z_q = 1$. It is clear that in the regions where the LO cross section diverges, large contributions from higher orders can be expected.

The dijet cross section including higher order parton emissions are difficult to calculate using exact expressions for the coefficient functions. Since the phase space integrals cannot be solved analytically, numerical methods have to be applied. Recently several Monte Carlo integration programs computing the cross section to next-to-leading order (NLO) became available. Early attempts like PROJETS⁵ or DISJET⁶ used a semi-analytical approach which only allowed jets to be defined by the W algorithm with the JADE scheme⁷ and were restricted to a small set of calculable distributions. Moreover, in these programs approximations were made which turned out not to be valid over the full phase space⁸. The programs MEPJET⁸, based on a phase space slicing method⁹, and DISENT¹⁰, based on a method to subtract the

^cThe polar angle is defined with respect to the incoming parton direction.

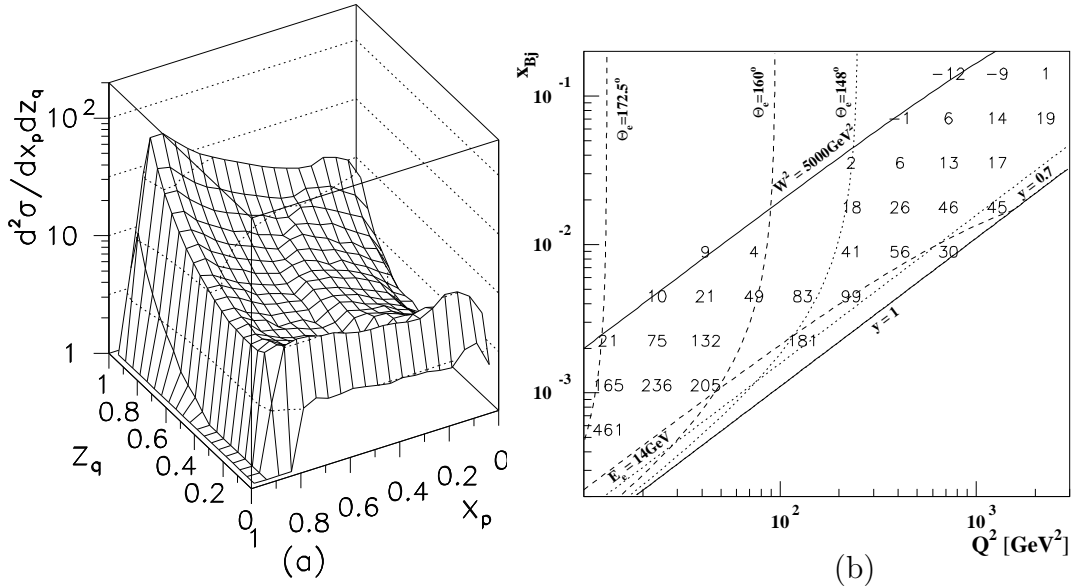


Fig. 3. a) Differential cross section $d^2\sigma/dx_p dz_q$ in first order of α_s for $x = 10^{-3}$ and $Q^2 = 10 \text{ GeV}^2$. The figure is taken from ref.³. b) Relative change in percent of the dijet rates when adding to the leading order cross section higher orders based on a leading logarithm parton shower model in the LEPTO Monte Carlo. The lines represent typical selection cuts on the scattered electron. In addition, a cut on $z_q > 0.1$ has been applied. The jet rate is based on the JADE algorithm for $y_{cut} = 0.02$. The figure is taken from ref.⁴.

divergences from individual contributions¹¹ and on an analytical treatment of specific divergent terms¹², are flexible NLO Monte Carlo programs which allow any jet definition scheme and arbitrary experimental cuts to be analyzed. For $Q^2 > 40 \text{ GeV}^2$ and for jets defined by the k_T algorithm¹³ the agreement of the $2 + 1$ and $3 + 1$ jet cross sections between the two programs is found to be on the 3% level¹⁴.

Higher order parton emissions and models for the transition of partons into hadrons are only included in Monte Carlo programs incorporating coefficient functions to leading order such as ARIADNE¹⁵, LEPTO¹⁶, HERWIG¹⁷, PYTHIA¹⁸ and RAPGAP¹⁹. They model multi-parton emission by either parton showers²⁰ (PS) based on the DGLAP equations or by a chain of independently radiating colour dipoles²¹ (CDM). HERWIG uses the cluster hadronisation model²². In all other programs hadronisation is based on the LUND string model²³ as implemented in JETSET²⁴.

The relative change in percent of the dijet rates defined with the JADE algorithm for $y_{cut} = 0.02$ when adding to the LO cross section higher orders based on a leading logarithm parton shower model (MEPS) is shown in Fig. 3 in the $x - Q^2$ plane applying typical analysis cuts on the scattered electron. While for $Q^2 > 100 \text{ GeV}^2$, the relative change only exceeds 20% in the low x region, parton showers change the dijet rate by a large factor for $10 < Q^2 < 100 \text{ GeV}^2$ and $1 \cdot 10^{-4} < x < 2 \cdot 10^{-3}$.

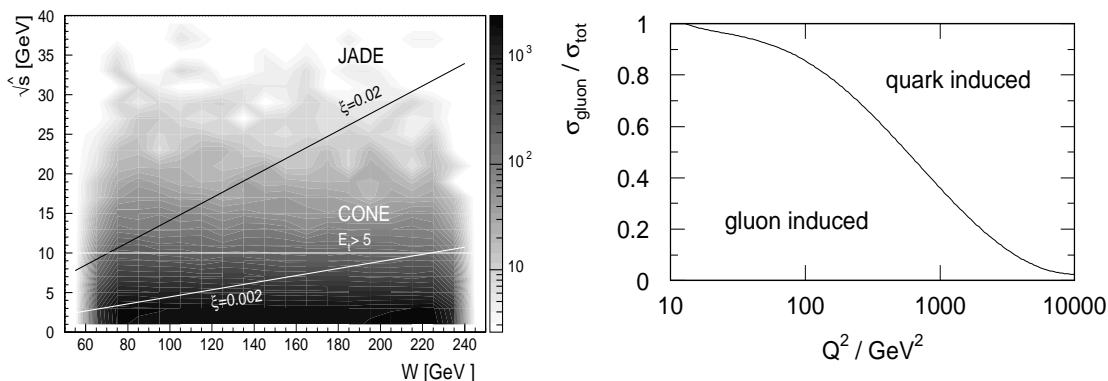


Fig. 4. a) Rate of 2 + 1 jet events as function of the invariant mass of the two jet system $\sqrt{\hat{s}}$ and the invariant mass of the hadronic final state W . Indicated are the phase space restrictions introduced when using the cone or the JADE algorithm. b) Fraction of gluon and quark induced processes leading to 2 + 1 jet events with $E_T > 5$ GeV and $-1 < \eta < 2$ defined by a K_t algorithm in the Breit frame as function of Q^2 . The cross section has been calculated in NLO in the kinematic range $x > 1 \cdot 10^{-4}$ and $0.15 < y < 0.65$.

The influence of parton emissions beyond leading order does also depend on the jet variables z_q and ξ . Since different jet algorithms cover different phase space regions, it is always important to specify which jet definition scheme was used. Fig. 4 illustrates the rate of 2 + 1 jet events as function of the invariant mass of the jet system $\sqrt{\hat{s}}$ and the invariant mass of the whole hadronic final state W . The rate rapidly increases towards low $\sqrt{\hat{s}}$. Indicated as lines are the phase space boundaries introduced by the JADE and the cone algorithm. With a cut on the transverse energy of the jets $E_T > 5$ GeV the minimum $\sqrt{\hat{s}}$ which can be reached is 10 GeV, since (in the limit of massless partons) from $E_T^2 = \hat{s} z_q (1 - z_q)$ follows $\sqrt{\hat{s}}/2 > E_T$. When using the JADE algorithm with a resolution parameter $d_{ij}/W^2 \approx \hat{s}/W^2 \approx \xi$, low values of $\sqrt{\hat{s}}$ can only be reached for low (high) values of W (x). If one takes $y_{cut} = 0.02$, $\sqrt{\hat{s}}$ is below 10 GeV for $W \lesssim 70$ GeV. The JADE algorithm with a high resolution parameter is therefore more restrictive than the cone algorithm. In addition to the region of low $\sqrt{\hat{s}}$, where collinear and infrared divergences become important, it naturally avoids the region of high W (low x) where a large phase space for multi-parton emission is available. However, the divergences at small and large z_q can only be avoided by a large y_{cut} .

Multi-jet production allows a variety of quantitative tests of our understanding of QCD dynamics. In a phase space region where the data are well described by perturbative QCD, HERA offers the opportunity to extract α_s over a wide range of Q^2 in a single experiment. This can be done at large x and Q^2 where the parton densities in the proton are well constrained. At low Q^2 and correspondingly low values of ξ , gluon initiated processes become increasingly important. Here, the measured 2 + 1 cross section can be used to determine the gluon density assuming a value of α_s . The sensitivity to both α_s and $g(\xi, Q^2)$ could also be used to simultaneously

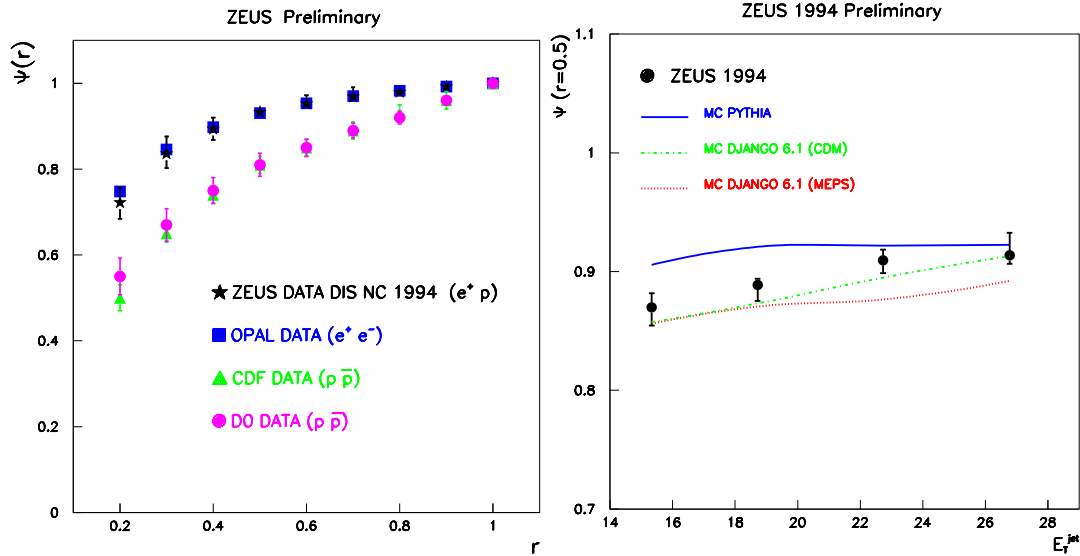


Fig. 5. a) Fractional transverse energy $\Psi(r)$ in a jet defined by a cone algorithm with radius $R = 1$ and $37 < E_t < 45$ GeV in the laboratory frame as function of $r = \sqrt{\Delta\eta^2 + \Delta\phi^2}$. For OPAL jets with $E_T > 35$ GeV were selected, for CDF (D0) the considered E_T range of the jets is $40(45) < E_T < 60(70)$ GeV. b) $\Psi(r = 0.5)$ as function of the transverse energy of the jet. QCD Monte Carlo models are superimposed. They either calculate the dijet cross section in LO and add multi-gluon emissions based on the colour dipole model (CDM) or by parton showers (MEPS) or treat QCD effects only by parton showers (PYTHIA).

extract these quantities. Such an analysis is however theoretically and experimentally difficult. In the region where the data significantly differ from what is expected by a fixed order calculation of perturbative QCD, jet observables are useful tools to gain insights in the complex parton dynamics occurring in electron proton collisions.

2. Jet shapes in DIS

The internal structure of jets provides useful information on the transition of a parton to the complex aggregate of hadrons which can be observed in the detector. The capability to describe detailed properties of jets is also an important ingredient when comparison of perturbative calculations with experimental data.

To study the internal structure of jets in the sample of neutral current DIS events with $Q^2 > 100$ GeV² jets are found in the laboratory system using the CDF-cone algorithm²⁵ with a cone radius $R = \sqrt{\Delta\eta^2 + \Delta\phi^2} = 1$. Only jets are considered which have in the laboratory frame a transverse energy $E_T > 14$ GeV and lie in the rapidity range $-1 < \eta < 2$. The jet shape is defined as the average fraction of the transverse energy of the jets inside an inner cone r concentric to the outer jet cone with radius R :

$$\Psi(r) = \frac{1}{N_{\text{jet}}} \sum_{\text{jets}} \frac{E_T(r)}{E_T(R)}, \quad E_T(r) = \int_0^r dr' dE_T(r')/dr' \quad (4)$$

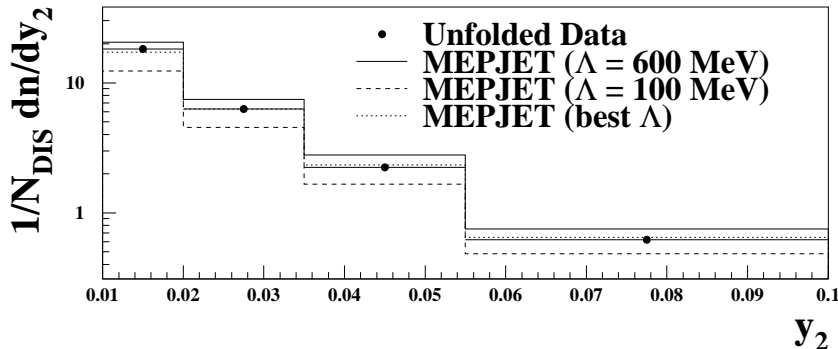


Fig. 6. Distribution of the resolution parameter y_2 in the JADE algorithm where a $1 + 1$ jet event switches to a $2 + 1$ jet event. Shown are unfolded data and the next-to-leading order prediction for some values of $\Lambda_{QCD}^{(4)}$. N_{DIS} is the total number of DIS events in the considered kinematic region.

where $E_T(r)$ is the transverse energy within an inner cone of radius r and N_{jet} is the total number of selected jets. By definition $0 < \Psi < 1$ and $\Psi(R) = 1$. The steepness of the rise of Ψ describes the collimation of the jet.

The jet shape Ψ corrected to hadron level for jets with $E_T > 37$ GeV as function of r is shown in Fig. 5a. 90% of the jet transverse energy is already contained in a cone with $r = 0.4$ around the jet axis. This is very similar to jets produced in e^+e^- collisions²⁶ with $E_T > 35$ GeV. The jets selected from $p\bar{p}$ collisions for $40 (45) < E_T < 60 (70)$ GeV measured by CDF (D0)^{27,28} are considerably broader. This might be explained by the fact that in e^+e^- and ep collisions the partons initiating the cascade leading to the jet are mainly quarks while in $p\bar{p}$ collisions they are gluons.

The jet shape depends on the transverse energy of the jet. Jets get narrower with increasing E_T as is shown in Fig. 5b.

Monte Carlo models based on a hard subprocess in LO plus additional multi-gluon emissions are able to describe the data. Also PYTHIA where QCD effects are only treated by parton showers reproduces the main features of the data. The best description of the E_T dependence of Ψ is obtained when partons are emitted according to the colour dipole model. The internal jet structure in DIS at HERA is fairly well reproduced by all QCD models.

3. Determination of the strong coupling constant

The $2 + 1$ jet rate defined with the JADE algorithm depends on the jet resolution parameter y_{cut} . For each event y_2 is defined as the value of y_{cut} where a $1 + 1$ jet event switches to a $2 + 1$ jet event.

A region of phase space is selected where NLO QCD can provide a reasonable description of the data, and where effects from multi-gluon emissions are small. In

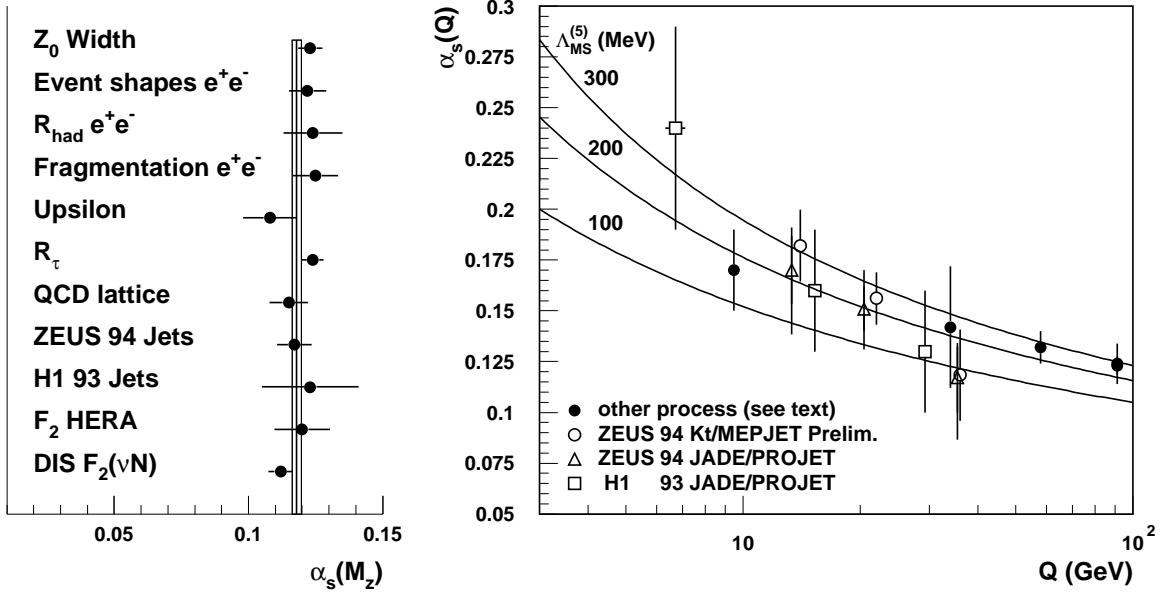


Fig. 7. Left: Values and total error of $\alpha_s(M_Z)$ from various processes. The solid line indicates the world average and the band its total error. Right: $\alpha_s(Q)$ from HERA (open symbols) and other processes with increasing Q (closed circles): Γ_Υ and $\sigma_{had}/\sigma_{tot}$, event shapes and $\Gamma_{hadron}/\Gamma_{lepton}$ in e^+e^- . The preliminary points using the k_T algorithm include the statistical errors only. The predictions of the renormalisation group equation for three values of $\Lambda_{\overline{MS}}$ are superimposed as lines.

the H1 analysis²⁹ this region is defined by: $Q^2 > 200 \text{ GeV}^2$ and $W^2 > 5000 \text{ GeV}^2$. To avoid events where the invariant mass of the two jet system is small and where the cross-section diverges, y_2 is restricted to $y_2 > 0.01$. The y_2 distribution, corrected to parton level by an unfolding method³⁰, is shown in Fig. 6. Overlaid is the prediction of NLO QCD for three values of α_s (respectively Λ_{QCD}). In all bins a strong sensitivity to α_s is observed. For one given value of α_s NLO QCD gives an excellent description of the data. The precision which can be expected from this measurement is of the order of $\Delta\alpha_s(M_Z)/\alpha_s(M_Z) \approx 5 - 10\%$.

Keeping $y_{cut} = 0.02$ fixed, the number of 2 + 1 jet events (N_{2+1}) normalized to the sum of 1 + 1 and 2 + 1 jet events ($N_{2+1} + N_{1+1}$) can be measured and is sensitive to α_s . Only jets in the acceptance region of $10^\circ < \theta_{jet} < 145^\circ$ and with $z_q > 0.1$ are counted. The fractional jet rate $R_2 = N_{2+1}/(N_{1+1} + N_{2+1})$ can be expressed by:

$$R_2(Q^2, y_{cut}) = A(Q^2, y_{cut}) \alpha_s(Q^2) + B(Q^2, y_{cut}) \alpha_s^2(Q^2) \quad (5)$$

From the coefficients A and B which can be calculated in NLO QCD and the measured R_2 , $\alpha_s(Q^2)$ can be extracted in different Q^2 bins. Using the renormalisation group equation these independent measurements can be used to fit $\alpha_s(M_Z)$.

For this measurement only the kinematic range of high Q^2 and high x is considered in order to reduce the uncertainties stemming from higher order gluon emissions and

from the hadronisation of a complex partonic configuration. The theoretically and experimentally difficult region towards the proton remnant is excluded. Three values of $\alpha_s(Q^2)$ extracted by the H1³¹ and ZEUS³² collaboration are shown in Fig. 7. For increasing values of Q^2 , $\alpha_s(Q^2)$ decreases as predicted by the renormalisation group equation shown for $\Lambda_{\overline{\text{MS}}}$ between 100 and 300 MeV (solid lines). An extrapolation to $\alpha_s(M_Z)$ yields:

$$\begin{aligned} \text{H1 93 :} \quad & \alpha_s(M_Z) = 0.123 \pm 0.012 \text{ (stat)} \pm 0.013 \text{ (syst.)} \\ \text{ZEUS 94 :} \quad & \alpha_s(M_Z) = 0.117 \pm 0.005 \text{ (stat)} \pm 0.005 \text{ (exp.)} \pm 0.007 \text{ (th.)} \end{aligned}$$

which is consistent with other values obtained from a large variety of different processes as shown in Fig. 7 (for ref. see³³). The agreement found in e^+e^- , ep and $p\bar{p}$ collision for reactions at very different scales is an important and successful test of QCD. The error on the HERA measurements are even with the present limited statistics already competitive. The dominant experimental errors stem from the uncertainty on the energy scale for hadrons, the model dependence of assigning partons to jets and the phenomenological description of the hadronisation process. Furthermore the renormalisation scale and the choice of the input parton density systematically influences the result. These results have been obtained with the NLO program PROJET or DISJET.

When particles are combined to jets, the details of how the 4-momenta are added are important, in particular, because higher order QCD calculations are only carried out for massless partons whereas the jets acquire a mass during the combination procedure. In the E-scheme 4-momenta are added to massive jets while in the E_0 and P -schemes jets remain massless by rescaling either the 3-momenta or the energy (see table 1 for details). The dependence of the jet cross section on the recombination schemes (RS) only appears in the calculation when jets are composed out of more than one parton. Corrections of $\mathcal{O}(\alpha_s^3)$ due to the different recombination schemes are potentially large. When applying different recombination schemes to the data, the measured 2+1 jet cross sections defined with the E and E_0 algorithms agree within few percent, but are lowered by up to 20% for the P -scheme³⁴. In PROJET only the E scheme is implemented. It is therefore not surprising that the extracted $\alpha_s(M_Z)$ agrees within 3% when the E and E_0 scheme is only applied to the data, but gives an inconsistent result when using the P scheme³⁴. An additional problem is that in the NLO calculation the W algorithm is implemented, while in the experimental analysis the JADE algorithm has to be used, i.e. mass terms in d_{ij} are neglected.

The new NLO programs MEPJET and DISJENT reveal a strong dependence on the recombination scheme³⁵ when using the JADE or W algorithm. In addition lead these algorithms to large NLO corrections of the dijet cross section.

The cone or k_T jet algorithms seem to be better suited for precision QCD tests, since the variation of the cross section when going from leading to next-to-leading order is much smaller³⁶. Moreover, these jet algorithms are less dependent on the

choice of the renormalisation and factorisation scale and allow a larger phase space to be covered.

The ZEUS collaboration has reanalyzed their data³⁷ using the k_T algorithm. The preliminary values of $\alpha_s(Q)$ obtained in three bins of Q are shown^d in Fig. 7. They are consistent with the results obtained with the JADE algorithm. The value extrapolated to the Z^0 boson mass is: $\alpha_s(M_Z) = 0.118 \pm 0.008$ (stat).

4. Determination of the gluon density

The parton distributions are well constrained for larger x where a lot of data are available. However, for low x , where gluons play a crucial rôle, they are not well known. In this regime, HERA has the unique possibility to investigate the distribution of the gluon density in the proton. The scaling violation of the proton structure function F_2 offers an indirect way to get a handle on the gluon density. This measurement^{38,39} is possible because of the extremely successful description of F_2 by the NLO DGLAP equations. Observables based on $2 + 1$ jet event can - by including them in the global analysis - provide a further constraint on the gluon density. Dijet rates can be calculated in next-to-leading order and are sensitive to the gluon density, since for $10 \lesssim Q^2 \lesssim 100$ GeV² the $2 + 1$ jet cross section is dominated by gluon initiated processes. In this kinematic region less than about 20% of the $2 + 1$ jet events are induced by quarks (see Fig. 4).

An alternative approach is to only base the analysis on the $2 + 1$ jet rate. Since large invariant jets masses ($\hat{s} > 100$ GeV²) are experimentally required to define clean jets, the very low x regime can not be reached. These measurements are nevertheless important to fill the gap between the results from small- x scaling violations in F_2 and the data on direct photon and jet production in $p\bar{p}$ collisions reaching to large- x ⁴⁰.

The H1 collaboration⁴¹ has already exploited the $2 + 1$ jet production to extract the gluon density in LO in the range $2 \cdot 10^{-3} \lesssim \xi \lesssim 0.18$. When processes where only one gluon is involved are considered, ξ is directly observable and the determination of $g(\xi, Q^2)$ is straight forward. This is however only of limited theoretical interest, since the LO dijet cross section is subject to large higher order corrections. There is moreover a large dependence on the arbitrary choice of the renormalisation and factorisation scale. Only, in NLO a reliable prediction of the dijet cross section is possible. The $2 + 1$ jet cross section, for instance, defined with a cone algorithm for jets with $E_T > 5$ GeV remains constant within 5% when varying the scale by 3 orders of magnitude while in LO variations of 40% are calculated³⁶.

A NLO extraction of $g(\xi, Q^2)$ requires, however, an iterative procedure where the input gluon density used in the NLO calculation is adjusted until the theoretical dijet cross sections agree with the measurement. This is most efficiently done by expanding the gluon density for a discrete set of points (ξ_1, \dots, ξ_n) using

^dOnly the statistical errors are included in the figure.

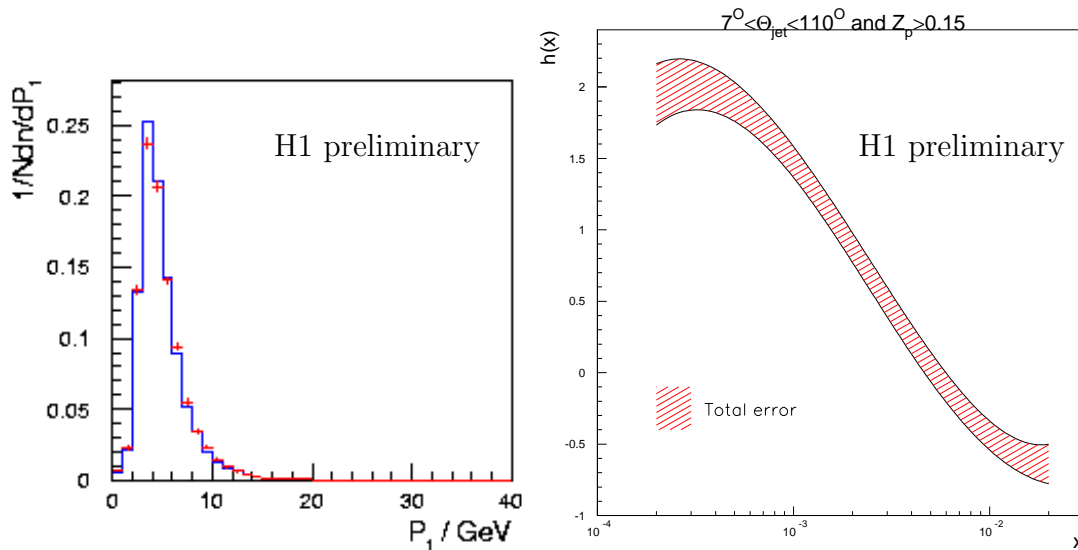


Fig. 8. Left: Shape normalised distribution of the transverse energy of jets defined with the k_t algorithm (in the Breit frame) using $Q^2/2$ as resolution parameter. The data have not been corrected for detector effects. Superimposed is a simulation based on LEPTO. Right: The function $h(x)$ describing the non-perturbative contribution of the dijet cross section as defined in the H1 analysis to extract the gluon density in NLO.

appropriate test functions $g(\xi, Q^2) = \sum_{n=1}^{n_{max}} a(\xi_n, Q^2) T_n(\xi)$ such that the integral $\sigma_g = \sum_{n=1}^{n_{max}} a(\xi_n, Q^2) \int d\xi/\xi C_{q\bar{q}}(x/\xi, Q^2) T_n(\xi)$ in equation 1 must only be calculated once. The coefficient a can then be used in the fitting procedure. Preliminary results using an elegant technique based on Mellin moments⁴², where the test functions take the form $T_n = (x/\xi)^n$, have been presented by the H1 collaboration³⁴ covering the range $0.01 < \xi < 0.1$ using the JADE algorithm.

Another approach also pursued by the H1 collaboration⁴³ is to use as test functions cubic splines⁴⁴ with the property $T_i(\xi_j) = \delta_{ij}$ and to introduce the $2 + 1$ jet rate as additional observable in a global fit analysis minimizing $\chi^2 = \chi^2(F_2) + \chi^2(R_{2+1}^{det})$. This has the advantage that no assumption on the quark densities is needed. The correlation of quarks and gluons via the DGLAP equation is naturally taken into account. R_{2+1}^{det} as measured in the detector is for each considered kinematic bin related to the NLO calculation of the dijet cross section σ_{2+1}^{pert} performed by DISENT:

$$R_{2+1}^{det} = \frac{MIG_{2+1}^{1+1} \cdot (\sigma_{2+1}^{pert}(x, Q^2) + h_{2+1}^{non-pert.}(x, Q^2))}{\sigma_{tot}(x, Q^2)} \quad (6)$$

The coefficients MIG_{2+1}^{1+1} correct for the migration of $1 + 1$ to $2 + 1$ jet events from hadron to detector level and can be determined using a fully simulated event sample based on LEPTO. The transition from partons to hadrons is modeled by a simple ansatz: $h_{2+1}^{non-pert.}(x, Q^2) = (\alpha + \beta \log x + \gamma \log^2 x + \delta \log^3 x)/Q^2$ When comparing NLO calculations to measurements, usually the data are ‘corrected to parton level’

by assuming that this transition is correctly described in a LO (improved by parton showers) Monte Carlo simulation program. To introduce a simple hadronisation model with additional free parameters in the fit procedure has the advantage that no a priori assumption on the underlying parton level is needed to relate the NLO calculation to the measurement. Recently, similar models based on power behaved terms⁴⁵ have been very successful in describing event shapes in DIS⁴⁶. In this context theoretical studies suggest that the terms $1/Q$ may also take into account multi-emissions of soft gluons associated with the behaviour of the running coupling constant at small scales⁴⁵.

In the kinematic range $25 < Q^2 < 100 \text{ GeV}^2$ and $2 \cdot 10^{-4} < x < 2 \cdot 10^{-2}$ jets are selected using the k_T algorithm with $d_{ij} = 0.5$ and Q^2 as scale. The jet rate for jets with $7^\circ < \theta_{jet} < 110^\circ$ and $z_q > 0.15$ is measured. LEPTO is able to describe the shape of most distributions associated to the hard subprocess. As an example Fig. 8 shows the E_T distribution of the jets as measured in the detector. LEPTO, however, fails to describe the absolute jet rate. The measurement is always about 20% above the predicted jet rate. This is true in the whole considered (x, Q^2) plane, but most pronounced for low Q^2 ($10 < Q^2 < 14 \text{ GeV}^2$) and low x ($2 \cdot 10^{-4} < x < 1 \cdot 10^{-2}$). The observed difference can not be accounted for by systematic effects. The most important systematic error of about 3 – 13% on the dijet rate is mainly due to the uncertainty of the hadronic energy scale.

The fit to the F_2 data and the jet rates leads to a good $\chi^2(R_{2+1}) = 10$ for 11 degrees of freedom, but no influence of the jet data on the extracted parton density functions is found in this analysis. Also the error band on the extracted gluon density is only marginally improved. This means that the extracted gluon density is essentially constrained by the inclusive F_2 data. The fitted non-perturbative function $h(x)$ is shown in Fig. 8. Without a strong x dependence of $h(x)$ no satisfactory fit can be performed.

A possible explanation of this results is that the way in which the k_T jet algorithm is used in this analysis leads to jets with relatively low transverse energy of 3 – 5 GeV (see Fig. 8) such that the found jet system does not always stem from the hard subprocess. Another explanation is that a fixed order calculation is not sufficient to account for the data in this phase space region. The difference between the NLO calculation and the data has therefore to be absorbed in the non-perturbative function $h(x)$ and consequently no sensitivity of the jet rates to the gluon density is found.

5. Comparison of jet rates to NLO-QCD

A similar observation about the incapability of NLO QCD to describe the dijet rates has been made by the ZEUS collaboration⁴⁷. In this study jets are selected using a cone algorithm in the laboratory frame requiring $E_T > 4 \text{ GeV}$ in the hadronic center of mass and the laboratory frame and excluding the forward region by $\eta_{lab} < 2$. The

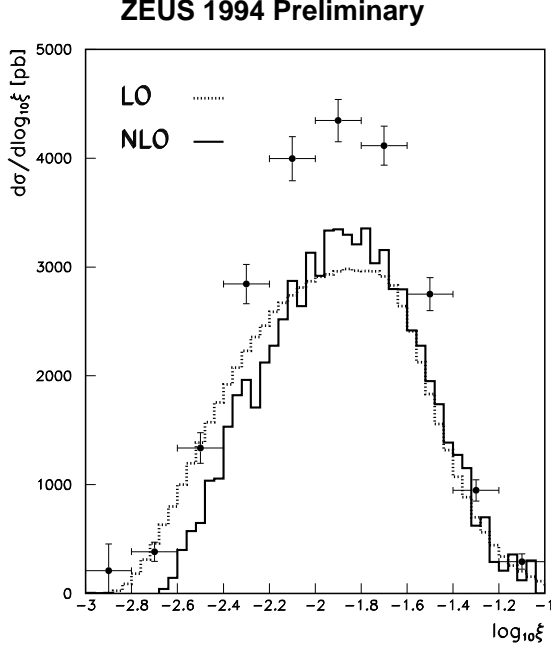


Fig. 9. $2 + 1$ jet rate cross section in function of the momentum fraction of the parton entering the hard subprocess ξ . Data have been corrected to parton level using the QCD Monte Carlo program LEPTO 6.3. Superimposed is a prediction from the QCD matrix element in LO and in NLO in α_s .

data are then corrected to parton level using LEPTO 6.3. The correction factors are between 1.2 and 1.8 for $4 \cdot 10^{-3} < \xi < 8 \cdot 10^{-2}$, but get very large (up to 3 – 4) for ξ around 10^{-3} . The shape of variables connected to the hard subprocess like E_T , η and ξ are well described by NLO programs. The absolute value of the $2 + 1$ cross section is, however, found to be about 30% higher in the data. This large difference cannot be explained by experimental effects like variation of the energy scale or the model dependence in the correction procedure nor by varying theoretical choices like different parameterizations of the parton densities or different factorisation and renormalisation scales.

That NLO QCD is not able to describe the dijet rates has recently been reported by the H1 collaboration^{48,49}. The dijet rate is measured with a cone algorithm using a cone radius $R = 1$ and requiring $E_T > 5$ GeV in the hadronic center of mass system. The rapidity difference between the two jets has to be $\Delta\eta < 2$. The $2 + 1$ jet rate corrected for detector effects is shown in Fig. 10 as function of x and Q^2 . NLO QCD (DISENT) as well as a conventional QCD model based on the exact LO coefficient functions plus additional DGLAP parton shower (RAPGAP ‘DIR’) clearly fail to describe the data. This is true for the whole kinematic range $5 \lesssim Q^2 \lesssim 100$ GeV² and $10^{-4} \lesssim x \lesssim 10^{-2}$, but is most pronounced in the low x and Q^2 region. In this region the prediction of the NLO QCD calculation is a factor of 2 higher than the QCD model, but is by the same factor below the data. Varying the input parton density

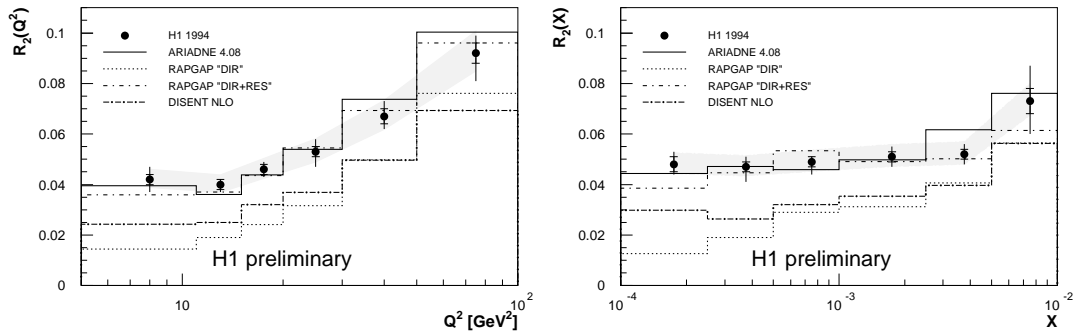


Fig. 10. 2 + 1 jet rates as function of Q^2 and x corrected to hadron level. Jets are defined by the cone algorithm with $E_T > 5$ GeV in the hadronic center of mass system. The difference in pseudorapidity between the two jets has to be smaller than 2. The band indicates the systematic error. Superimposed are the predictions from ARIADNE, a next-to-leading calculation (DISENT) and from RAPGAP (the direct and resolved contribution are shown separately).

functions leads to a change in the jet rate by up to 30%, but cannot account for the large discrepancy with the data.

The CDM model as implemented in ARIADNE is able to describe the data. In this model gluons are emitted from a chain of colour dipoles spanned between the current quark and the proton remnant. The first emission in the cascade is corrected by the matrix element to first order⁵⁰. It has been observed⁵¹ that quark induced processes have a up to a factor of 8 higher cross section than expected from conventional QCD, because the parton distribution functions in equation 1 are replaced by a phenomenological expression better adapted to the dipole picture. Partons with short wavelengths having high transverse momenta (P_T) only resolving part of the extended colour charge distribution of the proton remnant are suppressed by $(\mu/P_T)^\alpha$ where μ and α are phenomenological parameters usually set to 1. A similar suppression depending on the virtuality Q^2 is introduced in the direction of the scattered quark. It has been argued that the partonic state as encountered in ARIADNE is closely related to the one expected from a BFKL scenario⁵². In ARIADNE the hardest parton emission is not bound to the photon vertex, but can happen anywhere between the photon and the proton remnant.

Such a feature can also be artificially introduced in the conventional QCD model by assuming that the photon emitted from the incoming electron can fluctuate into quarks and gluons before entering the hard subprocess. This can be modeled by assuming a structure in the virtual photon like e.g. parameterized in the SaS model⁵³. Fig. 10 shows that adding this contribution (RAPGAP ‘RES’) to the processes where the photon is assumed to be point-like (RAPGAP ‘DIR’) does also reproduce the measured jet rate.

Only models where the hardest parton emission is not bound to occur at the photon vertex are able to describe the data. This indicates that in the phase space region tested by 2+1 jet production higher order processes which cannot be described by NLO QCD are important. Whether it is sufficient to simply add processes in the

photon direction without being in conflict with other HERA data, is not yet clear. The phenomenological treatment of higher orders in the colour dipole model has been proven to be extremely successful in describing all the data on the hadronic final state which have been measured at HERA^{54,55}. It remains however a puzzle why the shape of all distributions associated with the hard dijet system, like E_T , x_p , η etc., is well described by conventional QCD. It is hard to imagine that the importance of higher orders only affects the normalisation and not the shape of the distributions.

6. Conclusions

The understanding of jet production in DIS remains one of the main physics goals at HERA. While with the first HERA data, topics like the measurement of the strong coupling constant and the gluon density have been attacked with great enthusiasm, it turned out that these goals can only be achieved in a (very) restricted phase space region.

Existing data on jet production have always been tailored to a specific goal and present themselves today as a loose collection of scattered information. While conventional QCD is able to describe the data for $Q^2 > 100 \text{ GeV}^2$ and $\theta_{jet} > 10^\circ$ using the JADE algorithm, a discrepancy of about 30% is found for the low Q^2 region when using the cone or the k_T algorithm and excluding the forward region. The fully acceptance corrected jet rates in this region disagree by about a factor of two.

It seems that before precisely pinning down the strong coupling constant and the gluon density, one has to systematically investigate the applicability of NLO QCD in terms of kinematic phase space and the way how the jet observables are defined (jet algorithm, hard scale etc.).

In future, it will be necessary to measure jet cross sections corrected for detector effects extending to very low and very large x and Q^2 in order to find out where perturbative QCD is able to describe the data and where the mechanism governing jet production are more complicated. To achieve this goal the understanding of QCD models will play a major role.

7. Acknowledgements

I would like to thank my colleagues J. Dainton, G. Iacobucci, M. Kuhlen, E. Mirkes and M. Wobisch for their critical reading of the manuscript and helpful comments.

8. References

1. A. Mendez, Nucl. Phys. B145 (1978) 199; R. Peccei and R. Rückl, Nucl. Phys. B162 (1980) 125; C. Rumpf, G. Kramer and J. Willrodt, Z. Phys. C7 (1981) 337.
2. Y.L. Dokshitzer, Sov. Phys. JETP 46 (1977) 641; V.N. Gribov and L.N. Lipatov, Sov. J. Nucl. Phys. 15 (1972) 438 and 675; G. Altarelli and G. Parisi, Nucl. Phys. 126 (1977) 297.

3. A. Edin, G. Ingelman and J. Rathsman, *Z. Phys.* C75 (1997) 57.
4. K. Flamm, Phd thesis, University of Hamburg, DESY FH1-96-04 Hamburg, 1996.
5. D. Graudenz, *Phys. Lett.* B256 (1992) 518; *Phys. Rev.* D49 (1994) 3291; *Comp. Phys. Comm.* 92 (1995) 65.
6. T. Brodtkorb and J. G. Körner, *Z. Phys.* C54 (1992) 519; T. Brodtkorb and E. Mirkes, *Z. Phys.* C66 (1995) 141.
7. JADE Collab., W. Bartel et al., *Z. Phys.* C33 (1986) 23.
8. E. Mirkes and D. Zeppenfeld, *Phys. Lett.* B380 (1996) 205.
9. K. Fabricius, G. Kramer, G. Schierholz and I. Schmitt, *Z. Phys.* C11 (1981) 315; G. Kramer and B. Lampe, *Fortschr. Phys.* 37 (1989) 161; W.T. Giele, E.W.N. Glover, *Phys. Rev.* D46 (1992) 1980; W.T. Giele, E.W.N. Glover and D. A. Kosower, *Nucl. Phys.* B403 (1993) 663.
10. S. Catani and M. Seymour, *Nucl. Phys.* B485 (1997) 291.
11. R.K. Ellis, D.A. Ross and A.E. Terrano, *Nucl. Phys.* B178 (1981) 421.
12. S. Catani and M. Seymour, *Phys. Lett.* B378 (1996) 287.
13. S. Catani, Y.L. Dokshitzer and B.R. Webber, *Phys. Lett.* B285 (1992) 291.
14. E. Mirkes and D. Zeppenfeld, in: 5th Int. Workshop on DIS and QCD, eds. J. Repond and D. Krakauer, Chicago (USA) 1997.
15. L. Lönnblad, *Comp. Phys. Comm.* 71 (1992) 15.
16. G. Ingelman, in: *Physics at HERA*, eds. W. Buchmüller and G. Ingelman, Hamburg (Germany) 1991, Vol. 3, p. 1366; G. Ingelman, A. Edin and J. Rathsman, *Comp. Phys. Comm.* 101 (1997) 108.
17. G. Marchesini et al., *Comp. Phys. Comm.* 67 (1992) 465.
18. T. Sjöstrand, *Comp. Phys. Comm.* 82 (1994) 74.
19. H. Jung, *Comp. Phys. Comm.* 86 (1995) 147.
20. M. Bengtson and T. Sjöstrand, *Z. Phys.* C37 (1988) 465; M. Bengtson, G. Ingelman, T. Sjöstrand, in: *HERA Workshop 1987*, ed. R.D. Peccei, Hamburg (Germany) 1988, Vol. 1, p. 149.
21. G. Gustafson and U. Petterson, *Nucl. Phys.* B306 (1988); G. Gustafson, *Phys. Lett.* B175 (1986) 453; B. Andersson, G. Gustafson, L. Lönnblad and U. Petterson, *Z. Phys.* C43 (1989) 625.
22. B.R. Webber, *Nucl. Phys.* B238 (1984) 492.
23. B. Andersson et al., *Phys. Rep.* 97 (1983) 31.
24. T. Sjöstrand, *Comp. Phys. Comm.* 39 (1986) 347; T. Sjöstrand and M. Bengtsson, *Comp. Phys. Comm.* 43 (1987) 367, and for JETSET 7.3, T. Sjöstrand, CERN-TH-6488-92 (1992).
25. CDF Collab., F. Abe et al., *Phys. Rev.* D45 (1992) 1148.
26. OPAL Collab., R. Askers et al., *Z. Phys.* C63 (1994) 197.
27. CDF Collab., F. Abe et al., *Phys. Rev. Lett.* 70 (1993) 713.
28. D0 Collab., S. Abachi et al., *Phys. Lett.* B357 (1995) 500.
29. M. Weber, in: 5th Int. Workshop on DIS and QCD, eds. J. Repond and D. Krakauer, Chicago (USA) 1997.
30. V. Blobel, DESY 84-118, Hamburg 1984, and CERN Comp. School 1984.
31. H1 Collab., T. Ahmed et al., *Phys. Lett.* B346 (1995) 415.
32. ZEUS Collab., M. Derrick et al., *Phys. Lett.* B363 (1995) 201.
33. Particle Data Group, R.M. Barnett et al., *Phys. Rev.* D54 (1996).
34. K. Rosenbauer, in: *Workshop on DIS and Related Phenomena*, ed. G. D'Agostini and A. Nigro, Rome (Italy) 1996, p. 444.
35. E. Mirkes and D. Zeppenfeld, in: *Workshop on DIS and Related Phenomena*, ed. G. D'Agostini and A. Nigro, Rome (Italy) 1996, p. 428.
36. E. Mirkes and D. Zeppenfeld, *Acta Phys. Polon.* B27 (1996) 1393.
37. T. Trefzger, in: *Workshop on DIS and Related Phenomena*, ed. G. D'Agostini and A. Nigro, Rome (Italy) 1996, p. 434.

38. H1 Collab., S. Aid et al., Nucl. Phys. B470 (1996) 3.
39. ZEUS Collab., M. Derrick et al., Phys. Lett. B345 (1995) 576.
40. R.C.E. Devenish and A.D. Martin, in: Workshop on DIS and Related Phenomena, ed. G. D'Agostini and A. Nigro, Rome (Italy) 1996, p. 193.
41. H1 Collab., S. Aid et al., Nucl. Phys. B449 (1995) 3.
42. D. Graudenz et al. Z. Phys. C70 (1996) 77.
43. F. Zomer, in: 5th Int. Workshop on DIS and QCD, eds. J. Repond and D. Krakauer, Chicago (USA) 1997.
44. G. Lobo, in: 'Future Physics at HERA', eds. G. Ingelmann, A. De Roeck and R. Klanner, Hamburg (Germany) 1996, p. 537.
45. Y.L. Dokshizer and B.R. Webber, Phys. Lett. B352 (1995); R. Akhoury and V.I. Zakharov, Phys.Lett. B357 (1995) 646.
46. H1 Collab., C. Adloff et al., DESY 97-098, Hamburg, 1997.
47. D. Mikunas, in: 5th Int. Workshop on DIS and QCD, eds. J. Repond and D. Krakauer, Chicago (USA) 1997.
48. J. Spiekermann, in: XXXIIInd Rencontres de Moriond, ed. J. Tran Thanh Van, Les Arcs (France) 1997.
49. M. Wobisch, in: 5th Int. Workshop on DIS and QCD, eds. J. Repond and D. Krakauer, Chicago (USA) 1997.
50. L. Lönnblad, Z. Phys. C65 (1995) 285.
51. J. Rathsman, Phys. Lett. B393 (1997) 181.
52. L. Lönnblad, Z. Phys. C65 (1995) 285; A. H. Mueller, Nucl. Phys. B415 (1994) 373; J. Rathsman, Phys. Lett. B393 (1997) 181.
53. G. Schuler and T. Sjöstrand, Z. Phys. C68 (1995) 607 and Phys. Lett. B376 (1996) 193.
54. N. Brook et al., in: Future Physics at HERA, eds. G. Ingelman, A. DeRoeck and R. Klanner, Hamburg (Germany) 1996, Vol. 2, p. 613.
55. T. Carli, in: Workshop on Deep-Inelastic Scattering and Related Phenomena, ed. G. D'Agostini and A. Nigro, Rome (Italy) 1996 p.415.